

1 Frustration – induced inherent instability and
2 growth oscillations in pollen tubes

3 Mariusz Pietruszka*

Laboratory of Plant Physiology, Faculty of Biology and Environmental Protection

University of Silesia, ul. Jagiellońska 28, PL-40032 Katowice, Poland

tel. +48322009453, E-mail: mariusz.pietruszka@us.edu.pl

4 November 5, 2018

5 **Abstract.** In a seed plant a pollen tube is a vessel that transports male
6 gamete cells to an ovule to achieve fertilization. It consists of one elongated
7 cell, which exhibits growth oscillations, until it bursts completing its func-
8 tion. Up till now, the mechanism behind the periodic character of the growth
9 has not been fully understood. It is shown that the mechanism of pressure
10 – induced *symmetry frustration* occurring in the wall at the perimeter of
11 cylindrical and approximately hemispherical parts of a growing pollen cell,
12 together with the addition of cell wall material, suffices to release and sustain
13 mechanical self-oscillations and cell extension in pollen tubes. At the tran-
14 sition zone where symmetry frustration occurs and one cannot distinguish
15 either of the involved symmetries, a kind of 'entangled state' appears where
16 either single or both symmetry(ies) can be realized by the system. We antic-
17 ipate that testifiable predictions made by the model ($f \propto \sqrt{P}$) may deliver,
18 after calibration, a new tool to estimate turgor pressure P from oscillation
19 frequency f of the periodically growing cell. Since the mechanical principles
20 apply to all turgor regulated walled cells including those of plant, fungal and
21 bacterial origin, the relevance of this work is not limited to the case of the

*Corresponding author: mariusz.pietruszka@us.edu.pl

22 pollen tube.

23 **Keywords:** cell wall; equilibrium equation; frustration potential; growth
24 tensors; *Nicotiana tobaccum*; plant cytom mechanics

25 **1 Introduction**

26 **1.1 General outline**

27 The pollen tube has become a widely used cellular model system. In addition
28 to being the fastest growing plant cell, it features periodic oscillations of the
29 growth rate that have attracted numerous attempts to model the process¹.
30 While recent models have increasingly incorporated biological features such
31 as ion transport and intracellular trafficking, a simple feature with potentially
32 significant impact has been overlooked in past approaches: geometry. We
33 modeled the strain rates in the cell wall caused by turgor pressure depending
34 on the different symmetries present in the pollen tube and found that a
35 crucial area on the cellular surface of the pollen tube is characterized by
36 so termed *symmetry frustration*. This area represents the transition zone
37 between hemisphere-shaped apex and cylindrical shank. From a biological
38 point of view this zone is crucial since numerous molecular landmarks of
39 polar growth are present on one side of this zone and absent from the other.

40 The model predicts that the transition zone undergoes local peaks in
41 strain rate opening intriguing avenues for research focusing on the polarity of
42 the growth process. Furthermore, we propose that changes between different
43 symmetry regimes might be the mechanical underpinning of periodic changes
44 in growth rate and shape observed during oscillatory growth. We believe that
45 our model make an important contribution to the field of plant cytom mechanics
46 in general and pollen tube growth in particular.

¹The origin of this oscillation is still unclear, though all hypotheses agree in that, the cell wall mechanics are essential to the oscillation (Chavarria-Krauser and Yejie, 2011).

47 1.2 Preliminaries

48 Pollen tubes are rapidly growing plant cells whose morphogenesis is largely
49 determined by spatial gradients in the biochemical composition of the cell
50 wall. Pollen tube growth is a critical process in the life cycle of higher plants
51 (Winship et al., 2010). It has garnered a lot of attention and is at the center
52 of considerable controversy (Kroeger and Geitmann, 2011a). The pollen tube
53 is the carrier of the male gametes in flowering plants. A controversy swirls
54 around the modes of extension leading to periodicity in growth and growth
55 rate (Winship et al., 2010). While some authors claim that hydrodynamics
56 is the central integrator of pollen tube growth (Zonia and Munnik, 2007,
57 2009, 2011) leading to growth oscillations, the other couple the periodicity
58 in growth dynamics to the changes in the wall material properties (Winship
59 et al., 2010, 2011; Kroeger et al., 2011).

60 Pollen tubes are tip growing cells, which means that cell wall unidirec-
61 tional expansion is confined to the apex of the cell. They display extremely
62 rapid growth that can be also reproduced under *in vitro* conditions. All
63 growth activity - delivery of new cell wall material and cell wall deforma-
64 tion - occurs at the tip of the cell (Geitmann and Cresti, 1998): the tube
65 is capped by an approximately hemispherically shaped dome, the apex, to
66 which all growth activity is confined (Fig. 1A). The deformation is driven
67 by the turgor pressure, a hydrodynamic pressure inside the cell. Interest-
68 ingly, pollen tube evolution displays characteristic oscillations in growth and
69 growth rate (Plyushch et al., 1995; Hepler et al., 2001; Feijo et al., 2001).
70 The pollen tube (e.g. *Lilium longiflorum*, *Nicotiana tabacum*) growth oscil-
71 lation depends on many underlying phenomena, amongst others the ion and
72 mass fluxes, wall mechanical properties, system symmetry and turgor pres-
73 sure. In isotonic conditions (Zonia and Munnik, 2007) the average growth
74 cycle period T is about 50 s, while upon shifts to hypertonic or hypotonic
75 conditions it is about 100 s and 25 s, respectively. The latter produce oscil-
76 lations with typical frequencies ($f = 1/T$): hypertonic – 0.01 Hz, isotonic –
77 0.02 Hz and hypotonic – 0.04 Hz. The longitudinal and transversal oscillation
78 power spectrum of an individual *Nicotiana tabacum* pollen tube (Haduch and

79 Pietruszka, 2012) is visualized in Fig. 2, and can not solely be described by a
80 double exponent model (Pietruszka, 2012; e.g. Fig. 8A), suitable for normal
81 cell evolution, but incomplete for periodical growth.

82 The cell wall is one of the structural key players regulating plant cell
83 growth since plant cell expansion depends on an interplay between intra-
84 cellular pressures and the controlled yielding of the wall (Geitmann, 2009).
85 The cell wall may be treated as a polymer with the property of viscoelasticity
86 (colloquially "elasticity"), generally having notably low Young's modulus ϵ
87 and high yield strain, which is a normalized measure of deformation repre-
88 senting the displacement between particles in the body relative to a reference
89 length, compared with other materials. Cell wall polymers are amorphous
90 polymers existing above their 'glass' transition temperature, so that consid-
91 erable segmental motion is possible. At ambient temperatures, the cell wall
92 is thus relatively soft ($\epsilon \sim 1$ MPa) and easily deformed. Cells can grow to
93 some extent simply by stretching their walls as they take up water. However,
94 continued cell expansion involves synthesis of new wall material. Synthesis of
95 cellulose at the plasma membrane and pectin and hemicelluloses components
96 with Golgi apparatus deposits layers on the inside of the existing cell wall.
97 A mechanical prerequisite for the unidirectional growth of pollen tubes for
98 the (scalar) hydrostatic pressure is a softer cell wall at the tip of the cell,
99 and more rigid at the distal part (Geitmann and Steer, 2006; Fayant et al.,
100 2010). This gradient of mechanical properties is generated by the absence
101 or scarcity of callose and cellulose at the tip (Aouar et al., 2009) as well as
102 by the relatively high degree of esterification of the pectin polymers in this
103 region. The gradient in cell wall composition from apical esterified to distal
104 de-esterified is reported to be correlated with an increase in the degree of cell
105 wall rigidity and a decrease of visco-elasticity (Parre and Geitmann, 2005).
106 Also microindentation studies show (Fig. 2 in Winship et al., 2010) that
107 the pollen tube tip is less rigid and that the distal stiffness may be opposed
108 to apical softness. Needless to say, to sustain growth processes, a balance
109 between the mechanical deformation of the viscoelastic cell wall and the ad-
110 dition of new cell wall material must be achieved (Kroeger and Geitmann,
111 2011b).

112 Turgor pressure is the pressure of the cell sap against the wall in plant
113 cells. This is a force exerted outward on a plant cell wall by the water and
114 solutes contained in the cell. As a result it gives the cell rigidity. An ex-
115 cess turgor pressure or cell wall local weakening can result in the bursting
116 of a cell. Both constituents, turgor pressure and the wall properties are de-
117 cisive for the mechanical properties and dynamics of the developing plant
118 cell. The osmotically maintained (hydrodynamic) turgor pressure in living
119 plant cells and the mechanical properties of the cell wall itself are among
120 the most fundamental physical factors that dictate both cell growth and cell
121 morphogenesis in plants (Schopfer, 2006). In fact, the physical properties
122 of the wall and the turgor pressure have pivotal functions since they repre-
123 sent the 'downstream parameters' of all cellular signaling events (Chebli and
124 Geitmann, 2007). For our future purposes we note that turgor pressure is
125 high in pollen tubes: 0.1 – 0.4 MPa in lily (Benkert et al. 1997; Winship et
126 al., 2010).

127 The pollen tube geometry can be described by two different symmetries -
128 a hemisphere shaped apex, and a cylindrical shank zone, that are connected
129 by a transition zone between the two parts. In the present paper we propose a
130 mechanism of *symmetry frustration* occurring in this transition zone between
131 the two involved symmetries as a possible mechanism responsible for growth
132 rate oscillations. In simple terms by symmetry frustration we mean that a
133 small ring of cell wall (hereafter referred to as interface Γ , Fig. 1B) is unable
134 to 'decide' if it should behave as an elastic cylinder or an elastic sphere.
135 Following this hypothesis, oscillations may arise because this mesoscopic ring
136 behaves as if it 'jumps' periodically between the two mechanical states of
137 different capacity of strain energy.

138 The application of growth tensors to developing plant organs has been
139 known for a long time (Kutschera, 1989). Such mathematical description
140 has been utilized to apical meristems where the proliferating cells produce
141 tissue stresses, which in turn influence the structure of the developing organ
142 and, hence the principal directions of growth (Hejnowicz, 1984). A differ-
143 ent situation is observed for elongating plant organs, such as coleoptyles or
144 hypocotyles, or elongation zones in roots, where cell division rarely takes

145 place. Also, the directional evolution of a single cell is primarily observed for
146 the elongating pollen tube. As it may be expected, various stresses occur in
147 the elongating cell because of different properties of cell walls exposed to the
148 turgor pressure maintained by the gradient in the water potential (Kutschera,
149 2000). The distribution of the wall stresses as well as deformation of the par-
150 ticular wall layers can be calculated by solving equilibrium equations of elas-
151 ticity theory. Such equations may help to locate deformation of a cell wall,
152 exposed to an internal turgor pressure. The equilibrium equation may be
153 derived both for materials deformed elastically (deformation vanishes when
154 force equals zero) or non-elastically (plastic deformation survives, even when
155 the acting force is removed). In this article we concentrate initially on elastic
156 properties, because the highly controversial and uncertain mechanism of the
157 oscillatory growth of pollen tubes is our main concern² (Zonia and Munnik,
158 2011; Kroeger et al., 2011; Winship et al., 2011). Though, plastic properties
159 are inherently present in the proposed model *via* the derived (anharmonic)
160 'frustration potential', and the assumed cell wall building processes located
161 in the sub-apical, annular region, presumably at (about) the Γ – interface
162 (Zonia and Munnik, 2008; Geitmann and Ortega, 2009).

163 Possible mechanisms have been proposed to account for the oscillation of
164 pollen tube growth rate in quantitative terms (Bartnicki-Garcia et al., 2000;
165 Feijo et al., 2001; Dumais et al., 2006). A model for calcium dependent
166 oscillatory growth in pollen tubes has been put forward (Kroeger et al., 2008).
167 More recently the finite element technique was used (Fayant et al., 2010) to
168 establish biomechanical model of polar growth in walled cells. Also, the
169 chemically mediated mechanism of mechanical expansion of the pollen tube
170 cell wall by which deposition causes turnover of cell wall cross-links thereby
171 facilitating mechanical deformation was set forth (Rojas et al., 2011). The
172 role of wall ageing in self-regulation in tip-growth was considered in (Eggen et

²Whereas the hydrodynamic model as it is used by Zonia et al. proposes gradual increase in turgor until a threshold when rupture of individual links between cell wall polymers occurs, Winship and coworkers (Winship et al., 2010) state that turgor is essentially stable, but an exocytosis-induced relaxation of the wall causes expansion. They postulate that variations in cell wall mechanical properties cause the oscillations and that variations in turgor (if there are any) are a passive consequence due to cell wall relaxation.

173 al., 2011), while a model of plasma membrane flow and cytoskeleton regulation in
174 growing pollen tubes was discussed in (Chavarria-Krauser and Yeje, 2011).
175 The irreversible expansion of the cell wall during growth as the extension of
176 an inhomogeneous viscous fluid shell under the action of turgor pressure, fed
177 by a material source in the neighborhood of the growing tip was examined
178 in (Campas and Mahadevan, 2009). However, none of the models produced
179 oscillations on mechanical basis³.

180 In our approach, which does not contradict previous achievements, we
181 explore the relationship between turgor pressure and nontrivial cell geometry
182 by changing loss of stability picture (Wei and Linthilac, 2007) to encompass
183 cell wall mechanical properties in cylindrical and spherical geometries, both
184 present in rapidly extending pollen tube. We base our physical model on the
185 parametrized description of a tip growing cell that allows the manipulation of
186 cell size, cell geometries, cell wall thickness, and local mechanical properties.
187 However, the mechanical load (contrary to op. cit.) is applied in the form of
188 hydrostatic (constant) pressure.

189 An important feature of pollen tubes elongation is that growth rate oscil-
190 lates and, additionally, many of the underlying processes also oscillate with
191 the same period, but usually with different phase (e.g. Fig. 1c in (Zonia
192 and Munnik, 2011)). However, the role of the oscillating ion gradients and
193 fluxes in the control of pollen tube growth (Hepler and Winship, 2010) is
194 beyond the scope of this paper and we will not discuss it here. Nonetheless,
195 the outlined scenario leaves space for the periodical ion and mass fluxes in
196 and out of the cell. We also share the fundamental view expressed in (Rojas
197 et al., 2011; Proseus and Boyer, 2006) that the wall extension is primarily
198 a biophysical (mechanical) process, although ultimately dependent on enzy-

³The model presented by Chavarria-Krauser and Yeje (2011), actually does not describe the cell wall, and hence, does not predict oscillations. The authors simply assume that the growth oscillations are given to understand the phase angle differences between growth velocity and the regulating mechanisms. However, by definition, oscillation is the repetitive variation, typically in time, of some measure *about* a central value (often a point of equilibrium), and pollen tubes do not exhibit such form of oscillations. In fact, what we observe in pollen tubes is a periodical elongation (without shrinking phase), and can be a result of transitions between two or more different states, which is another definition of oscillation, which we adopt in this paper.

199 matic activity, and that under conditions where the enzymatic background
200 can be subtracted the biophysical process still proceeds normally.

201 Any new model should deliver testifiable and quantitative predictions
202 that can be validated by experimental data. In case of pollen tubes, it is
203 necessary to present predictions that go beyond stress values which are in-
204 herently difficult to measure. The presented model satisfies this requirement
205 offering, among others, an experimentally testifiable power law ($\omega \propto \sqrt{P}$)
206 between the turgor pressure P and growth oscillation angular frequency ω .

207 **2 Results and discussion**

208 In search for the cause of experimentally observed pollen tube growth oscilla-
209 tions we link analytic stress/strain relations with the mechanical properties
210 of a tip growing cell, located at the perimeter of hemispherical dome and
211 cylindrical shank. This is based on the observation that cell wall assembly
212 by exocytosis occurs mainly at an annular region around the pole of the
213 cell (Geitmann and Dumais, 2009; Zonia and Munnik, 2009) and that the
214 concomitant turgor driven deformation of the cell wall causes characteristic
215 strain in the hemisphere shaped apex of the cell (Fayant et al, 2010; Rojas
216 et al., 2011). The dynamical properties of such a complex growing system
217 should be found self-consistently (meaning that the turgor pressure and the
218 wall mechanical properties are conjugate magnitudes that usually form cou-
219 pled equations, which have to be solved by iteration methods). Nevertheless,
220 in first approximation the following heuristic solution can be proposed.

221 Assuming an intrinsic turgor pressure P , and a much smaller external
222 pressure, of yet unspecified origin p_{ext} (it can be just atmospheric pressure)
223 producing an effective pressure $\tilde{P} = P + p_{\text{ext}}$ the equilibrium equation for
224 the displacement vector \vec{u} , which is the shortest distance from the initial to
225 the final position of a moving point, takes the form (Landau and Lifshitz,
226 1986):

$$2(1 - \nu) \text{grad}(\text{div} \vec{u}) - (1 - 2\nu) \text{curl}(\text{curl} \vec{u}) = \vec{0} \quad (1)$$

227 where ν is the Poisson coefficient, which is the ratio, when a sample ob-

228 ject is stretched, of the contraction or transverse strain, to the extension
 229 or axial strain. From now on Young modulus $\epsilon(z)$ and Poisson coefficient ν
 230 are assumed as picewise constant functions, so they remain constant on the
 231 interface Γ .

232 Note, that by acting divergence operator on both sides of Eq. (1) we re-
 233 ceive $\Delta \operatorname{div} \vec{u} = 0$, i.e. $\operatorname{div} \vec{u}$ denoting the volume change due to displacement
 234 field is a harmonic function satisfying Laplace's equation.

235 Eq. (1) may be solved analytically, providing that a problem exhibits a
 236 high degree of symmetry. In particular it can be solved exactly for spherical
 237 and cylindrical symmetries. Both symmetries are present in the description of
 238 pollen tube self-similar elongation, since the distal part resembles cylindrical
 239 tube while the apex is a hemispherical dome (Fig. 1B). Thus, the symmetries
 240 present in both subdomains should be utilized in the description of pollen
 241 tube shape and dynamical properties.

242 By assuming cylindrical symmetry (for the displacement vector field $\vec{u} =$
 243 $(u_r, u_\phi, u_z) = (u_r, 0, 0)$, which is obtained under the assumption that the
 244 total length of the cylinder part remains constant (the axial elongation of
 245 the more rigid shank upon application of a constant internal pressure P we
 246 assume as negligible), and hence we accept $u_z = 0$ in the Ansatz $(u_r, u_\phi, u_z) =$
 247 $(u_r, 0, 0)$ instead of $(u_r, u_\phi, u_z) = (u_r, 0, u_z)$, which would lead to unavoidable
 248 numerical solution of Eq. (1)), and representing field operators (grad, div
 249 and curl) in cylindrical (polar) coordinates, Eq. (1) can be reduced to a much
 250 simpler form:

$$\frac{d}{dr} \left[\frac{1}{r} \frac{d}{dr} (r u_r) \right] = 0. \quad (2)$$

251 This differential equation can be solved for the displacement field u_r to yield
 252 the displacement for the cylindrical symmetry

$$u_r^c = ar + \frac{b}{r}, \quad (3)$$

253 where a and b are constants to be determined from the boundary conditions
 254 (Landau and Lifshitz, 1986). Also, by introducing spherical coordinates with
 255 the origin in the center of a sphere the displacement field \vec{u} is a function of

256 the radius r : $\vec{u} = (u_r, u_\theta, u_\phi) = (u_r, 0, 0)$. Therefore $\text{rot } \vec{u} = 0$ and Eq. (1)
 257 reads: $\text{grad div } \vec{u} = 0$. Hence, for the spherical symmetry we receive for
 258 displacement

$$u_r^s = ar + \frac{b}{r^2}, \quad (4)$$

259 where the upper index in Eqs (3) and (4) has been substituted to differenti-
 260 ate solutions for cylindrical (c) and spherical (s) geometries. The geometry
 261 of the elongating pollen tube can be described with a cylinder of radius r_T
 262 capped by a half prolate spheroid with short radius r_T and a long radius r_L
 263 (see e.g. Fig. 1a in (Fayant et al., 2010)). Thus, as a model for normally
 264 growing tube we propose a thin-walled hollow cylinder ended by a hemispher-
 265 ical shell immersed in an external pool of pressure p_{ext} and filled with a cell
 266 sap with turgor pressure P (we equate both radii $r_T = r_L$, for simplicity).
 267 The inner radius of the cylinder and a sphere is r_1 , while the outer radius
 268 is r_2 (Fig. 1B). Another simplifying assumption of the model is that we
 269 deal with weak (elastic) interactions at the interface Γ , due to wall building
 270 processes occuring at this region, and hence the deflection field may slightly
 271 differ on both sides (from the mechanical point of view they may be treated
 272 as weakly coupled). It is consistent with the view that deposition chemically
 273 loosens the wall by breaking load-bearing cross-links while simultaneously
 274 creating new, load-free cross-links, thereby effecting a fail-safe scenario for
 275 mechanical expansion (Rojas et al., 2011).

276 Based on the proposition that the mechanical cell wall properties at the
 277 growing tip must be different from those in the shank, it was suggested
 278 (Dumais et al., 2004; Kroeger et al., 2008) that an anisotropy in the cell
 279 wall elasticity is required to account for the transition between spherical
 280 and tubular shape at the tip of the cell. Also, it was found (Geitmann and
 281 Parre, 2004) that the rigidity of the tip of the pollen cell was an increasing
 282 function of the distance from the apex. Therefore, the elastic properties
 283 of the cylinder imitating the cell wall at the shank and the hemispherical
 284 tip are represented by two pairs of material constants: Young's modulus ϵ ,
 285 also known as the tensile modulus, which is a measure of the stiffness of an
 286 elastic material and is a quantity used to characterize materials, and Poisson

287 coefficient ν . In further calculations, we assume different values for these
 288 coefficients for distal (thick and rigid) and apical (thin and elastic) walls
 289 of a pollen tube. Such assumptions, about different values of mechanical
 290 constants at the apical dome and cylindrical shank, are fully justified (see
 291 e.g. Fig. 4 in (Geitmann and Parre, 2004) , where a spatial distribution
 292 of the Young’s modulus is presented). Because we consider relatively small
 293 elastic deformations, the stress and strain tensors are related by the Hooke’s
 294 law of elasticity (which is an approximation that states that the extension of
 295 a spring is in direct proportion with the load applied to it) and makes the
 296 deformation reversible. For the radial part of the stress tensor σ_{ij} we have:
 297 $\sigma_{rr} = -p_{\text{ext}}$ at $r = r_2$ and $\sigma_{rr} = -P$ at $r = r_1$. Since the off-diagonal elements
 298 vanish, we are left with the strain $u_{rr} = \frac{du_r}{dr} = a - \frac{b}{r^2}$, $u_{\phi\phi} = \frac{u_r}{r} = a + \frac{b}{r^2}$ and
 299 $u_{zz} = 0$, the interesting radial σ_{rr} element of the stress tensor reads⁴:

$$\sigma_{rr} = \frac{\epsilon}{(1 + \nu)(1 - 2\nu)} \left[a - (1 - 2\nu) \frac{b}{r^2} \right]. \quad (5)$$

300 By assuming boundary conditions as above, parameters a and b can be cal-
 301 culated (Lewicka and Pietruszka, 2009). They both depend on material con-
 302 stants: Young’s modulus ϵ and Poisson coefficient ν , cylinder geometry (r_1 ,
 303 r_2 – radii) and pressure values P and p_{ext} .

304 Quantitative calculations stemming from Eqs (3) – (5) are presented in
 305 Figs 3 – 4. In Fig. 3A we observe (a) lowering of deformation u_r with
 306 radius r of apical hemispherical shell (b) almost constant u_r for a thin-walled
 307 cylinder. This fact produces a wall stress presented in Fig. 3B equal to
 308 about 60 MPa (for the model parameters), which seems big enough to cause
 309 cell wall instability at Γ – interface⁵. The calculated wall stress of the order

⁴In fact, to receive smooth solutions on Γ – interface equations for different geometries should be connected by transmission (gluing) conditions equating the forces and deflections on each side: $\sigma \mathbf{n} = \sigma' \mathbf{n}'$ and $\mathbf{u} = \mathbf{u}'$, where \mathbf{n} denotes the exterior normal to the boundary. In first approximation we let both subdomains be weakly coupled (visco – plastic phase) while cyclic wall building processes take place at Γ , and strongly coupled mechanically (visco – elastic phase) when wall building processes expire. We consider only the radial part of the stress σ_{rr} , deflection u_r and strain $u_{rr} = \partial_r u_r$ tensors on Γ , for simplicity. This Ansatz, however, does not qualitatively influence the results.

⁵Typical plant cell turgor pressures in the range of 0.3 to 1.0 MPa translate into between 10 and 100 MPa in the walls (Wei and Linthilac, 2007).

310 of tenths of MPa is enough to cause local wall instability (radial strain),
 311 subsequent axial relaxation, wall building and unilateral cell expansion at the
 312 interface between the hemispherical apex and cylindrical shank. Unavoidable
 313 repetition of this process, owing to a constant effective pressure and a positive
 314 feedback mechanism necessary to drive oscillations (to overcome damping
 315 due to viscosity), may generate observable oscillations which continue until
 316 the wall building processes expire. Depending on the wall thickness, the
 317 calculated stress is equal to the distance between the curves (a) and (b)
 318 (inset). The tensile stress difference calculated at the apex and the distal
 319 part of the pollen tube cell wall ($\sigma_{rr}(\text{apex}) - \sigma_{rr}(\text{distal})$) is shown in Fig. 3C.
 320 Here it is parametrized by the turgor pressure P acting on the cell wall. The
 321 tensile stress in the wall clearly rises, as we increase the turgor pressure –
 322 this would, in turn, cause an increased growth oscillation frequency, as it is
 323 observed experimentally in the transition from hypertonic, through isotonic
 324 to hypotonic conditions (Zonia and Munnik, 2007).

325 The influence of turgor on the oscillation period, as predicted by the
 326 model described in (Kroeger and Geitmann, 2011a), is also in agreement
 327 with our results presented in Fig. 4A and their consequences: the higher the
 328 pressure, the higher the oscillation frequency. Tensile stress difference at the
 329 transition zone, parametrized by the wall thickness, is presented in Fig. 4B.

330 From the expression for tensile stress difference due to the symmetry
 331 change (note, curvature discontinuity and stress singularity occur at the tran-
 332 sition zone) $\sigma_{rr}^c - \sigma_{rr}^s \equiv \sigma_{rr}(\text{cylinder}) - \sigma_{rr}(\text{sphere})$ which equals

$$\sigma_{rr}^c - \sigma_{rr}^s = P \left[\frac{r_1^3 r_2^3}{r^3 (r_2^3 - r_1^3)} - \frac{r_1^2 r_2^2}{r^2 (r_2^2 - r_1^2)} - \frac{r_1^3}{r_2^3 - r_1^3} + \frac{r_1^2}{r_2^2 - r_1^2} \right] \quad (6)$$

333 and from the opposite formula: $\sigma_{rr}^s - \sigma_{rr}^c$, it is shown that calculations per-
 334 formed for an infinitesimally narrow ring Γ , where both geometries (cylin-
 335 drical and spherical) intervene, a *symmetry frustration* – leading to oscilla-
 336 tions of the radial part of the stress tensor – may take place. ‘Frustration’
 337 originates from the fact that none of the locally involved symmetries is dis-
 338 tinguished. On the other hand, the calculated from Eq. (6) (by evaluating

339 $E = \int \sigma_{rr} dr$) strain energy density reads:

$$E_{\pm} \propto \pm P \frac{r_1^2 r_2^2 [2r^3 + 2r(r_1^2 + r_1 r_2 + r_2^2) - r_1 r_2 (r_1 + r_2)]}{2r^2 (r_1^4 + r_1^3 r_2 - r_1 r_2^3 - r_2^4)} \quad (7)$$

340 The quasi-discrete energy levels E_- and E_+ (possesing, however, a small
341 dispersion $\delta E \cong 0.0003$ [energy u.]) presented in Fig. 5 are non-degenerate
342 due to the existence of a constant turgor pressure P which leads to the
343 observed splitting (see also upper inset). Still, since both levels originate
344 from the symmetry change at the critical limit considered in this work, they
345 can be attributed to the oscillations in the pollen tube growth functions.
346 Thus, the *resonating frequency* of growth (growth rate) corresponds to the
347 energy difference $E_+ - E_- \cong 2E$ (since $E_+ \cong -E_-$), which in turn is directly
348 proportional to the turgor pressure P . Consequently, we may equate the
349 transition energy $2E$ between the resonating levels (Fig. 5) with pollen tube
350 oscillation frequency observed in experiments (Eq. (7) implies that if $P = 0$
351 then the system exhibits no oscillations, which is exactly the case, see also
352 the plot of the potential energy $U(r)$ at $r = r_0$ in Fig. 6).

353 Notwithstanding, we note that the considered effect is exclusively con-
354 nected with geometrically induced stress in the wall which may be linked
355 with symmetry frustration⁶, and one can express it in measurable units [Pa
356 m]. Indeed, calculating definite integral over the function expressed by Eq.
357 (6): $\int_{r_1}^{r_2} [\dots] dr$ (with $r_1 = 5$ and $r_2 = 5.25 \mu\text{m}$) we receive the strain energy
358 density: $E_{\pm} = \pm 0.256$ [MPa μm]. Therefore, the difference of strain energy
359 density between the two levels is about 0.5 MPa for micrometer length scales
360 typical for the width (which is about 250 nano-meters) of the pollen tube cell
361 wall. Such energy density may lead to oscillations which are observable not
362 only in growth rates. From our model it can also be deduced that the apical
363 geometry oscillates (due to deformation u_r located initially at Γ , compare
364 Figs 3B and 4B in Pietruszka et al., 2012) to produce the so called pearled
365 morphology (Rojas et al., 2011). Relicts (residues) of such deformations at

⁶A spatially degenerate ground state will undergo a geometrical distortion (the alteration of the original shape) that removes that degeneracy, because the distortion lowers the overall energy of the whole complex.

366 Γ are traced in Fig. 1c and 6a, c (ibid.) as crests smeared out on a distance
 367 λ , in agreement with our model⁷. However, what else draws our attention
 368 is that there is no sign of deflections at a distance shorter than the tube ra-
 369 dius R . The latter observation further supports the main idea presented in
 370 this paper of specific role of the Γ – interface in initiating oscillations. By
 371 assuming, after Rojas et al. (2011), the value of the linear $v_{\text{avg}} = 0.2$ [$\mu\text{m/s}$]
 372 of the elongating cell and taking the average oscillation period $T = 50$ s
 373 from Fig. 7 we receive the observed wavelength of about $\lambda = 10$ [μm], which
 374 is a doubled value of the radius R , as it should be expected assuming the
 375 correctness of our approach. In this picture, the distance λ comprise the
 376 local deflection/wall stress/stress relaxation/recovery through wall building
 377 processes for every period T .

378 Transitions between the states of different symmetry are shown in Fig. 5.
 379 The system is pumped with energy to jump over the analytic discontinuity
 380 (energy gap) between the (hemi-)spherical and cylindrical geometry. As a
 381 positive feedback mechanism necessary to drive the oscillations (to prevent
 382 damping due to viscosity) the energy is absorbed (ATP–pumping (Rounds
 383 et al., 2011)) in the transition zone above the state E_- producing the exited
 384 state E_+ . Then the system returns (by spontaneous symmetry breaking, to
 385 reduce the energy of the overall system) to the lower symmetry (cylindrical)
 386 state E_- stimulating axial expansion. Both transitions (up and down) close
 387 one growth cycle with the predicted transition’s rate $\omega \propto \frac{2\pi}{T}$, where T is the
 388 period. The whole process is repeated at the expense of pressure P and
 389 ATP–energy needed for wall synthesis (exhibiting growth oscillations), and
 390 eventually expires or reaches critical instability (the cell bursts).

391 In a mechanical anharmonic oscillator, the relationship between force and
 392 displacement is not linear but depends upon the amplitude of the displace-
 393 ment. The nonlinearity arises from the fact that the spring (here: cell wall)
 394 is not capable of exerting a restoring force that is proportional to its dis-
 395 placement because of stretching in the material comprising the wall. As a

⁷Such geometrical oscillations of the wave-length λ will be obtained when frustration occurs, and the cylindrical and spherical symmetries will be present on Γ – contour interchangeably; compare Movie S1 and S2 in (Pietruszka et al., 2012).

396 result of the nonlinearity, the vibration frequency and amplitude can change,
 397 depending upon the system elements displacement upon pressure P . An ap-
 398 proximate derivation performed in Appendix 1 delivers the analytic form of
 399 the (dual) 'frustration potential', which is a sum of attractive and repulsive
 400 forces, possibly responsible for experimentally observed growth rate oscilla-
 401 tions in pollen tubes. The latter, which is given by Eq. (12) and visualized
 402 in Fig. 6, we describe here shortly: Pollen tube oscillations are trapped at
 403 the potential well about the equilibrium point r_0 for the corresponding sym-
 404 metric (harmonic) potential. Oscillation frequencies and amplitudes of the
 405 anharmonic potential depend upon the turgor pressure values, see Eqs (6)
 406 and (7), as it is observed (e.g. Fig. 4 in Kroeger et al., 2011; Kroeger and
 407 Geitmann, 2011a)). Wall expansion is allowed by molecular separation (r -
 408 values) exceeding those of harmonic potential. Dissociation energy at zero
 409 potential level corresponds to system instability (burst at Γ). The constant
 410 turgor pressure, as taken from Fig. 5, induces the value of $U(r)$, hence the
 411 frequency of the oscillation and its amplitude. The low-lying (trapped) values
 412 deliver high frequencies and small amplitudes, while the higher-lying poten-
 413 tial values - low frequencies and larger amplitudes of oscillations. Above the
 414 critical threshold (corresponding to 'zero energy' at the vertical scale) a bond
 415 breaking occurs and the pollen tube burst at the transition zone, or deliver
 416 male gametes completing its function. The lower plot represents only one
 417 branch (of the prevailing cylindrical symmetry) of the full frustration poten-
 418 tial; the second branch (above) is in 'dual' subspace, and the oscillations take
 419 place between both branches. For the negative values of the cylindrical sym-
 420 metry, as shown in the plot, the mechanism of symmetry breaking favors
 421 this 'lower order' (cylindrical) symmetry for cell extension.

422 The presented in Fig. 6 frustration potential is a more convenient model
 423 for vibrational structure of wall constituting molecules than harmonic oscilla-
 424 tor potential, because it explicitly includes the effects of bond breaking and
 425 accounts for anharmonicity of real bonds in the extending cell wall. It is
 426 also responsible for the inherent instability at the Γ - interface of a grow-
 427 ing tube (and - in consequence - polymer building process), which can be
 428 experimentally supported by the fact that the pollen tubes always rupture

429 at the transition zone where the radial part of the strain tensor is consid-
430 erable (Pietruszka et al., 2012, Movie S3). The form of the potential also
431 contributes to the long debate among plant physiologists about the elas-
432 tic/inelastic extension of plant cell wall in simple terms: any departure from
433 parabola centered around r_0 will lead to plastic extension, corresponding to
434 elongation growth (Fig. 6). In addition, the infinite potential barrier at low
435 distance r values prevents the growing cell wall from shrinking at a given
436 pressure P .

437 In order to calculate the value of the resonance angular frequency ω we
438 momentarily accept the approximate (classical) relation: $E \propto \omega^2$. Assuming
439 $P = 0.3$ MPa, taking the approximate A constant from the fit (see Fig.
440 7) we receive $f \cong 0.09$ Hz, a value which belongs to the observed frequency
441 spectrum in pollen tube growth functions (0.01 Hz – \sim 0.20 Hz, (Haduch and
442 Pietruszka, 2012) for tobacco, Fig. 2; and (McKenna et al., 2009) for lily).
443 As an aside, we stress that the calculated from Eq. (7) resonance frequency
444 satisfies a power law $\omega \propto \sqrt{P}$ (see Appendix 2 for detailed derivation). The
445 application of this important relation to the experimental data is presented in
446 Fig. 7. It is easy to notice, that this relation ($\omega = 2\pi A\sqrt{P}$, or equivalently
447 $f = A\sqrt{P}$, where A is a constant – connected with the wall mechanical
448 properties – to be determined from experiment, and $[P] = \text{MPa}$), if inverted,
449 can serve (after calibration) to estimate difficult to measure turgor pressure
450 P values from easy to measure oscillation frequencies (or periods T).

451 Furthermore, it is clear that the material properties of the cell wall in the
452 apical region should not be homogeneous, and therefore a proper mechanical
453 description of growth must involve a gradient in material properties from the
454 apical to the distal region (Fayant et al., 2010; Eggen et al., 2011). It has
455 been shown (Eggen et al., 2011) that the calculated "expansion propensity"
456 as a function of the distance from the apex measured in units of the tube
457 radius R (notation, as in (Eggen et al., 2011)) shrinks to an area near the
458 apex. Closer examination reveals that the inflection point is located at about
459 1 pollen tube cylinder radius R , a place where we perform our calculations.
460 The latter statement means that the slope is the greatest at $z \sim R$ (in axial
461 direction). This, and the fact that the 'dilution' sector is shown (Fig. 2 in

462 Eggen et al., 2011)) exactly at the limit of the two considered axisymmetric
463 zones, is consistent with the view of intense changes of the wall mechanical
464 properties at the limit of the distal and apical part. The 'dilution' effect is
465 caused in our model by a rapid surface expansion due to displacement u_r of
466 the Γ – interface (see also (Parre and Geitmann, 2005): Fig. 1 – a local dip
467 in the wall stiffness appears at about $10 \mu\text{m}$ from the apex, a place where
468 our calculations are performed; and Fig. 7 (2) showing the possible local-
469 ization of the transition zone from the cylindrical to spherical symmetry).
470 Corresponding radial strain may trigger exocytosis that results in delivery
471 of new cell wall material which rejuvenates this area. However, we should
472 note, what we observe is not only according to the mechanical properties
473 gradient, but mainly due to the changing symmetry at this place and the
474 analytical consequences (curvature discontinuity) of this fact (compare e.g.
475 Eqs 3 and 4). Likewise, observations, together with the analysis of Floures-
476 cence Recovery After Photobleaching (FRAP) experiments (Geitmann and
477 Dumais, 2009; Bove et al., 2008) indicate that exocytosis is likely to occur
478 predominantly in the same annular region (cf. (Geitmann, 2010), Fig. 1)
479 where wall expansion rates are greatest. It is concluded in the same work,
480 that tip growth in plant cells does not seem to happen exactly at the tip.
481 Further supporting data is provided in (Zonia and Munnik, 2008), where the
482 vesicle fusion with the plasma membrane was shown to approach to within
483 $2\text{-}5 \mu\text{m}$ distal to the apex. The observations that growth is mainly at an
484 annular region around the pole are in accord with calculations presented in
485 this article. Probing mechanical properties at the perimeter of cylindrical
486 and spherical part may result in calculation of the local rate of exocytosis
487 (the conventional explanation for this phenomenon, i.e. oscillating exocyto-
488 sis rate (see e.g. Fig. 4A in (Cardenas et al., 2008), Fig. 2 in (McKenna
489 et al., 2009), is widely accepted). This may be roughly estimated by taking
490 the oscillation frequency from Fig. 7. The read off value: $f \sim 0.02 - 0.03$
491 Hz is in accord with the main observed periodical mode (Zonia and Munnik,
492 2007) in the longitudinal power spectrum of pollen tube oscillatory motion,
493 and presumably may be equated with the rate of exocytosis and new cell
494 wall assembly in *Nicotiana tobaccum* pollen tubes and temporal variations in

495 the secretion of cell wall precursors (Kroeger and Geitmann, 2011a). This
 496 periodical growth activity, in turn, could be related (among others) to the
 497 relaxation of the stress (invoked by the hydrostatic turgor pressure) in the Γ
 498 – interface, i.e. in close proximity to the advancing apex of the cell, probably
 499 at the vesicle delivery zone in the subapex, where the vesicles are released
 500 into the cytoplasm (Fig. 3 in (Kroeger et al., 2009)). In addition, even
 501 small stress/strain fluctuations at this narrow cylindrical ring, belonging to
 502 both adjacent zones, localized on its circumference could lead to macrosopi-
 503 cally observable change of orientation of this ring and consequently direction
 504 change of the elongating pollen tube. This is indeed the case – see e.g. Fig.
 505 1F in (Zonia and Munnik, 2008), and even more pronounced in Fig. 1 in
 506 (Calder et al., 1997). It seems that polar growth in pollen tubes is associated
 507 with spatially confined dynamic changes in cell wall mechanical properties
 508 (Zerzour et al., 2009; and Appendix 2). Furthermore, the time course of an
 509 experiment, showing very little change in turgor pressure during cell growth,
 510 was measured by pressure probe monitoring of growing *Lilium longiflorum*
 511 (Winship et al., 2010, Fig. 1a) and re-analysed in (Zonia and Munnik, 2011,
 512 Fig. 3b-c). Even though direct measurements fail to indicate large-scale tur-
 513 gor changes during growth, rapid small-scale pressure changes (jumps) are
 514 visible, which presumably⁸ may be caused by the change of orientation of the
 515 tilt angles of wall building cellulose microfibrils in subsequent growth cycles
 516 in the considered transition zone⁹. As stated (ibid.), the measured periodic-
 517 ity for pressure oscillations ranges from 12 s to 25 s, which is the same as the
 518 routinely reported for oscillatory dynamics in lily pollen tubes (McKenna et
 519 al., 2009; Zerzour et al., 2009) and approximately agrees with the calculated
 520 frequency ($f = 1/12 \cong 0.09$ Hz) from our model (see next paragraph). Closer
 521 examination of Figs 3a-c in (Zonia and Munnik, 2011) reveals, in addition,
 522 a slight but steady diminishing of turgor (negative slope) which can be a

⁸There is, however, no evidence for cellulose microfibrils to be involved in small changes in turgor. These small jumps in turgor may be simply imprecisions in the measurement method. This method requires readjusting the meniscus in a pressure probe needle for each data point and the measurement is inherently associated with significant noise.

⁹The direction of maximal expansion rate is usually regulated by the direction of net alignment among cellulose microfibrils, which overcomes the prevailing stress anisotropy (Baskin, 2005).

523 consequence of cell volume expansion in every cycle. The latter observation
524 may be associated with the passive role of the turgor pressure in pollen tube
525 growth, at least at unchanging osmotic potentials. In conclusion, we agree
526 with the view, that in the growth process the (main) energy supply is de-
527 rived from turgor, while the growth rate and direction from the wall local
528 properties (Winship et al., 2010).

529 Expansive growth in a plant cell relies on the interplay between the inter-
530 nal turgor and the forces in the cell wall opposing deformation. Which of the
531 two parameters controls the dynamics of growth has been controversial in the
532 case of pollen tube growth (Zerzour et al., 2009). The long-standing model
533 of pollen tube growth considers that cyclic changes in cell wall properties
534 initiate growth (Holdaway-Clarke and Hepler, 2003; Winship et al., 2010).
535 A new model based on accumulating data from recent work indicates that
536 oscillations in hydrodynamic flow and intracellular pressure initiate growth
537 (Zonia 2010; Zonia and Munnik, 2011). Both models agree that once growth
538 initiated, osmotic pressure drives cell elongation. We have shown that the
539 rapid polar growth phases during oscillatory growth in pollen tubes may be
540 preceded by a strain – induced softening of the cell wall at the brink of the
541 apical and distal parts (Γ). We also showed that cellular turgor pressure does
542 not need to undergo changes during these repeated growth phases to display
543 periodicity in growth. However, turgor pressure still preserves an important
544 role, together with the cell wall mechanical properties, in controlling the dy-
545 namics of pollen tube growth by changing wall stress and hence oscillation
546 frequencies in the different osmotic environments – the frequency of oscilla-
547 tory pollen tube growth in our model can be altered by changing the osmotic
548 potential value of the surrounding medium (Kroeger and Geitmann, 2011a).

549 There are many observations of oscillations that could affect growth rates
550 (such as wall material deposition and extracellular ion fluxes). However, even
551 from purely mechanical calculations, performed at the boundary between the
552 wall cylinder shell and hemispherical shell at the apex, the following picture
553 for the sequence of events for the elongating pollen tube emerges. A given
554 (constant) turgor pressure produces *different* strain at the apical and distal
555 wall parts possessing various mechanical properties and different symmetries.

556 This phenomenon is especially important at the narrow interface between
557 these neighbouring parts. Consequently, a localized elevated stress of the
558 order of tenths MPa is invoked in the wall causing serious instability at the
559 brink of both sections generated by symmetry frustration, and the cell wall
560 relaxation (loosening) process takes place in order to reduce tensile stress.
561 This initiates a wall building process (which is an implicit assumption of the
562 model) in meridional direction. However, the effective turgor pressure pro-
563 duces strain at the similar location (in the co-moving – with the moving tip –
564 reference frame) axially equidistant from the tip and the whole process/cycle
565 repeats. This eventually results in time – periodicity in the growth dynamics
566 recognized in the literature as pollen tube oscillations.

567 **3 Final comment**

568 This article offers a nontrivial solution for a long – sought mechanism of
569 pollen tubes growth oscillations, which is the subject of swirling controversy
570 in the field. It is based on the phenomenon of *symmetry frustration* of the
571 cell wall in the apical region. This simple physical mechanism results in
572 analytically determined asymmetric 'frustration potential', the appearance of
573 the landscape of 'discrete' energy levels at (different) constant pressures and
574 the aforementioned oscillatory growth comes from the transitions between
575 them. Moreover, a scaling relation between the turgor pressure P and the
576 angular frequency of the oscillations ω is derived, which is represented by a
577 power 1/2 – law ($\omega \propto \sqrt{P}$). Later on, this prediction is successfully verified
578 against a real plant physiological experimental data.

579 **Acknowledgements**

580 Author thank dr Paweł Gusin, string theory specialist, Institute of The-
581 oretical Physics, University of Wrocław, Poland and Professor dr hab. Jan
582 Sładkowski, Department of Astrophysics and Cosmology, Institute of Physics,
583 University of Silesia, Katowice, Poland for critical reading of the manuscript.
584 I feel specially indebted to David Logan, Coulson Professor of Theoretical

585 Chemistry Oxford University, Physical and Theoretical Chemistry, Oxford,
 586 United Kingdom for expressing his kind opinion and encouragement about
 587 this work.

588 Appendix 1

589 (i) The local force equation of motion in the mechanics of continuous bodies
 590 (due to Cauchy) reads (Lublimer, 2006):

$$\partial_j \sigma_{ij} + F_i = 0, \quad (8)$$

591 where $i, j = 1, 2, 3$, and Einstein's summation convention is used. By ignoring
 592 any possible shear stresses and assuming for the infinitesimally small Γ -
 593 interface $\sigma_{\phi\phi} = 0$ and $\sigma_{zz} = 0$

$$\sigma_{ij} = \begin{pmatrix} \sigma_{rr} & 0 & 0 \\ 0 & \sigma_{\phi\phi} & 0 \\ 0 & 0 & \sigma_{zz} \end{pmatrix} \simeq \begin{pmatrix} \sigma_{rr} & 0 & 0 \\ 0 & 0 & 0 \\ 0 & 0 & 0 \end{pmatrix} \quad (9)$$

594 we receive $\sigma_{rr} = \sigma(r)$, which is the only matrix element that survives. From
 595 Eq. (8) we have

$$\int \partial_j \sigma_{ij} dx^i + \int F_i dx^i = 0 \quad (10)$$

596 so since $\int F_i dx^i = -U(x)$ is the potential energy then $\int \partial_j \sigma_{ij} dx^i = U(x)$.
 597 Hence in our case $\int \partial_r \sigma_{rr} dr = \sigma_{rr} = U(r)$, and one gets: $U(r) = \sigma_{rr} = \sigma(r)$.

598 (ii) By identifyng

$$U(r) = \sigma(r) \quad (11)$$

599 we may follow Eq. (6) to receive

$$\Delta \sigma^\pm = \pm \frac{\alpha}{r^3} \mp \frac{\beta}{r^2} + C \quad (12)$$

600 where $\alpha = P \frac{(r_1 r_2)^3}{r_2^3 - r_1^3}$, $\beta = P \frac{(r_1 r_2)^2}{r_2^2 - r_1^2}$ and C is a constant. Next, in order to find

601 r_0 we write $\Delta\sigma'(r_0) = 0$ to get

$$-\frac{3\alpha}{r^4} + \frac{2\beta}{r^3} = 0 \quad (13)$$

602 Hence

$$r_0 = \frac{3\alpha}{2\beta}. \quad (14)$$

603 Since $U \equiv \Delta\sigma$ we can plot the 'symmetry frustrated' potential $U(r)$, Fig. 6.
604 (iii) Considering small oscillations around equilibrium r_0 , we may introduce
605 new coordinate ρ : $r = r_0 - \rho$ and by substituting it to Eq. (12) receive

$$U(x) = \frac{1}{r_0^3} \frac{\alpha}{(1-x)^3} - \frac{1}{r_0^2} \frac{\beta}{(1-x)^2} \quad (15)$$

606 where $x = \rho/r_0$. By expanding both fractions for small x , we finally get the
607 form for the harmonic potential:

$$U(x) = \frac{4\beta^3}{9\alpha^2} x^2 - \frac{4\beta^3}{27\alpha^2} \quad (16)$$

608 Comparing the above equation with the classical oscillator potential ($m = 1$):
609

$$U(x) = \frac{1}{2}\omega^2 x^2 + U_0 \quad (17)$$

610 and using Eq. (12) we get $\omega^2 \propto P$.

611 Hence, the pollen tube oscillation frequency at the limit of small oscillations
612 equals $\omega \propto \sqrt{P}$, where P is the turgor pressure (compare also with Fig.
613 7, where the proportionality constant (A) is estimated from experiment).

614 **Appendix 2**

615 Pollen tube oscillation: local deflection/wall stress/relaxation/recovery

616

617 STAGES of one oscillation (mechanical view):

- 618 1. Recovery through wall building at Γ – interface: visco-plastic process
619 (elastic equations do not apply here, because of wall and mass pro-

620 duction; the system is merely plastic and both subdomains are weakly
621 coupled from the mechanical point of view).

622 2. Strain and deformation production on Γ (the equations apply).

623 3. Wall stress production on both sides of Γ and the resulting strain en-
624 ergy: visco-elastic process (equations apply).

625 4. Elastic strain energy relaxation in one cycle to produce elongation of
626 one wave length (compare Rojas et al, 2011, Fig. 1C, Fig 6A): the
627 phenomenology applies $f = A\sqrt{P}$, finding confirmation in comparison
628 with authors' (Haduch and Pietruszka, 2012) performed experiment,
629 Fig. 7. The process repeats: next oscillation takes place (go to 1. to
630 start another oscillation).

631 References

- 632 [1] Aouar L, Chebli Y, Geitmann A (2009) Morphogenesis of complex plant
633 cell shapes - the mechanical role of crystalline cellulose in growing pollen
634 tubes. Sexual Plant Reprod 23: 15-27
- 635 [2] Azuah RT, Kneller LR, Qiu Y, Tregenna-Piggott PLW, Brown CM, Cop-
636 ley JRD, Dimeo RM (2009) DAVE: A comprehensive software suite for the
637 reduction, visualization, and analysis of low energy neutron spectroscopic
638 data. J Res Natl Inst Stan Technol 114, 341
- 639 [3] Bartnicki-Garcia S, Bracker C, Giertz G, Lopez-Franco R, Lu H (2000)
640 Mapping the growth of fungal hyphae: orthogonal cell wall expansion dur-
641 ing tip growth and the role of turgor. Biophys J 79: 2382-2390
- 642 [4] Baskin T (2005) Anisotropic Expansion of the Plant Cell Wall. Annu Rev
643 Cell Dev Biol 21: 20322
- 644 [5] Benkert R, Obermeyer G, Bentrup FW (1997) The turgor pressure of
645 growing lily pollen tubes. Protoplasma 198: 1-8

- 646 [6] Bove J, Vaillancourt B, Kroeger J, Hepler P, Wiseman PW, Geitmann A
647 (2008) Magnitude and direction of vesicle dynamics in growing pollen tubes
648 using spatio-temporal image correlation spectroscopy (STICS). *Plant Phys*
649 147: 1646-1658
- 650 [7] Calder A, Franklin-Tong VE, Shaw PJ, Drobak BK (1997) Ca^{2+} oscil-
651 lations in plant cells: initiation by rapid elevation in cytosolic free Ca^{2+}
652 levels. *Biochem Biophys Res Commun* 29: 690-694.
- 653 [8] Campas O, Mahadevan L (2009) Shape and dynamics of tip-growing cells.
654 *Curr Biol* 19: 2102-2107
- 655 [9] Cardenas L, Lovy-Wheeler A, Kunkel JG, Hepler PK (2008) Pollen tube
656 growth oscillations and intracellular calcium levels are reversibly modu-
657 lated by actin polymerization. *Plant Physiology* 146: 1611-1621
- 658 [10] Chavarria-Krauser A, Yejie D (2011) A model of plasma membrane flow
659 and cytoskeleton regulation in growing pollen tubes. *J Theor Biol* 285: 10-24
- 660 [11] Chebli Y, Geitmann A (2007) Mechanical principles governing pollen
661 tube growth. *Funct Plant Sci Biotech* 1: 232-245
- 662 [12] Dumais J, SR Long, and SL Shaw (2004) The mechanics of surface
663 expansion anisotropy in *Medicago truncatula* root hairs. *Plant Phys* 136:
664 3266-3275
- 665 [13] Dumais J, Shaw S, Steele C, Long S, Ray P (2006) *Int J Dev Biol* 50,
666 209-222
- 667 [14] Eggen E., Keijzer MN, Mulder BM (2011) Self-regulation in tip-growth:
668 the role of cell wall ageing. *J Theor Biol* 283: 113-121
- 669 [15] Fayant P, Girlanda O, Chebli Y, Aubin CE, Villemure I, Geitmann A
670 (2010) Finite element model of polar growth in pollen tubes. *Plant Cell*
671 22: 2579-93

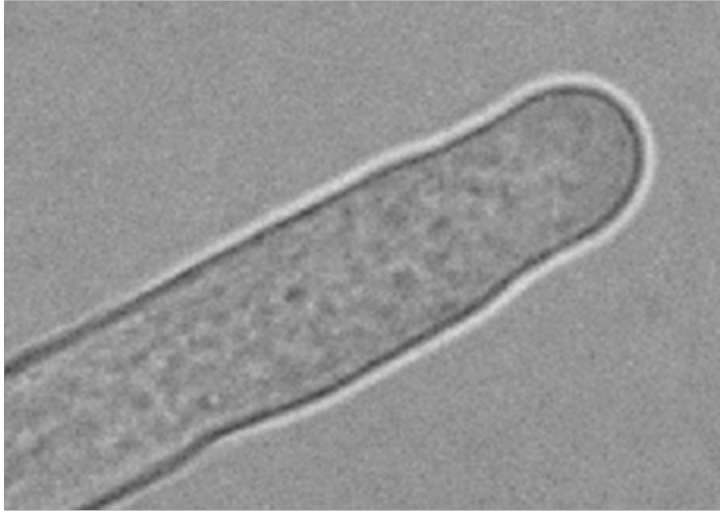
- 672 [16] Feijo JA, Sainhas J, Holdaway-Clarke TL, Cordeiro MS, Kunkel JG,
673 Hepler PK (2001) Cellular oscillations and the regulation of growth: the
674 pollen tube paradigm. *BioEssays* 23: 86-94
- 675 [17] Geitmann A, Cresti M (1998) Ca^{2+} channels control the rapid expan-
676 sions in pulsating growth of *Petunia hybrida* pollen tubes. *J Plant Phys*
677 152: 439-447.
- 678 [18] Geitmann A, Parre E (2004) The local cytomechanical properties of
679 growing pollen tubes correspond to the axial distribution of structural
680 cellular elements. *Sex Plant Reprod* 17:9-16
- 681 [19] Geitmann A, Steer MW (2006) The architecture and properties of the
682 pollen tube cell wall. In the pollen tube: A cellular and molecular perspec-
683 tive, *Plant Cell Monographs*, R Malho, ed (Berlin, Heidelberg: Springer
684 Verlag), pp. 177-200
- 685 [20] Geitmann A (2009) How to shape a cylinder - Pollen tube as a model
686 system for the generation of complex cellular geometry. *Sex Plant Reprod*
687 23: 6371
- 688 [21] Geitmann A, Dumais J (2009) Not-so-tip-growth. *Plant Signaling &*
689 *Behavior* 4: 136-138
- 690 [22] Geitmann A, Ortega JKE (2009) Mechanics and modelling of plant cell
691 growth. *Trends Plant Sci* 14: 467-478
- 692 [23] Geitmann A (2010) Mechanical modeling and structural analysis of the
693 primary plant cell wall. *Current Opinion Plant Biol* 13: 693-699
- 694 [24] Haduch A, Pietruszka M (2012) Power spectrum, growth velocities and
695 cross-correlations for longitudinal and transversal oscillations of *Nicotiana*
696 *tabacum* pollen tube – *J Exp Bot*, under review / asking for resubmission.
697 Also: Power spectrum of *Nicotiana tabacum* pollen tube. *Int Conf Biophys*
698 *Stud*, 18.05-20.05.2012, Kraków, Poland
- 699 [25] Hejnowicz Z (1984) Trajectories of principal directions of growth, natu-
700 ral coordinate system in growing plant organ. *Acta Soc Bot Pol* 53: 29-42

- 701 [26] Hepler PK, Vidali L, Cheung AY (2001) Polarized cell growth in higher
702 plants. *Annu Rev Cell Dev Biol* 17: 159-187
- 703 [27] Hepler PK, Winship LI (2010) Calcium and the cell wall - cytoplasm
704 interface. *J Int Plant Biol* 52: 147-160
- 705 [28] Holdaway-Clarke, TL, Hepler PK (2003) Control of pollen tube growth:
706 role of ion gradients and fluxes. *New Phytol* 159: 539-563
- 707 [29] Kroeger JH, Geitmann A, Grant M (2008) Model for calcium dependent
708 oscillatory growth in pollen tubes. *J Theor Biol* 253: 363-374
- 709 [30] Kroeger JH, Daher FB, Grant M, Geitmann A (2009) Microfilament ori-
710 entation constrains vesicle flow and spatial distribution in growing pollen
711 tubes. *Biophys J* 97: 1822-1831
- 712 [31] Kroeger JH, Zerzour R, Geitmann A (2011) Regulator or driving force?
713 The role of turgor pressure in oscillatory plant cell growth. *PLoS One* 6:
714 e18549
- 715 [32] Kroeger J, Geitmann A (2011a) Modeling pollen tube growth: feeling
716 the pressure to deliver testifiable predictions. *Plant Signaling & Behavior*
717 6: 1828-1830
- 718 [33] Kroeger J, Geitmann A (2011b) Pollen tube growth: get-
719 ting a grip on cell biology through modeling. *Mech Re Comm*,
720 doi:10.1016/j.mechrecomm.2011.11.005
- 721 [34] Kutschera U (1989) Tissue stresses in growing plant organs. *Physiol*
722 *Plant* 77: 157-163
- 723 [35] Kutschera U (2000) Cell expansion in plant development. *R Bras Fisiol*
724 146: 126-132
- 725 [36] Landau LD, Lifshitz EM. *Theory of Elasticity*. Vol. 7 (3rd ed.).
726 Butterworth-Heinemann, 1986.

- 727 [37] Lewicka S, Pietruszka M (2009) Mathematical model of tissue stresses
728 in growing plant cells and organs. *Acta Soc Bot Pol* 78: 19-23
- 729 [38] Lubliner J. *Plasticity theory*. Pearson Education, Inc., Revised ed. 2006
- 730 [39] McKenna ST, Kunkel JG, Bosch M, Rounds CM, Vidali L, Winship
731 LJ, Hepler PK (2009) Exocytosis precedes and predicts the increase in
732 growth in oscillating pollen tubes. *Plant Cell* 21, 3026-3040
- 733 [40] Parre E, Geitmann A (2005) Pectin and the role of the physical prop-
734 erties of the cell wall in pollen tube growth of *Solanum chacoense*. *Planta*
735 220: 582-592
- 736 [41] Pietruszka M (2012) A biosynthesis/inactivation model for enzymatic
737 WLFs or non-enzymatically mediated cell evolution. *J Theor Biol* 315:
738 119-127
- 739 [42] Pietruszka M, Lipowczan M, Geitmann A (2012) Persistent sym-
740 metry frustration in pollen tubes. *PLoS ONE* 7(11): e48087.
741 doi:10.1371/journal.pone.0048087
- 742 [43] Plyushch, T.A., Willemse, M.T.M., Franssen-Verheijen, M.A.W., and
743 Reinders, M.C. (1995) Structural aspects of in vitro pollen tube growth
744 and micropylar penetration in *Gasteria verrucosa* (Mill.) H. Duval and
745 *Lilium longiflorum* thumb. *Protoplasma* 187: 13-21
- 746 [44] Proseus TE, Boyer JS (2006) Identifying cytoplasmatic input to the cell
747 wall of growing *Chara corallina*. *J Exp Bot* 57: 3231-3242
- 748 [45] Rojas ER, Hotton S, Dumais J (2011) Chemically mediated mechanical
749 expansion of the pollen tube cell wall. *Biophysical J* 101: 1844-1853
- 750 [46] Rounds CM, Winship LJ, Hepler PK (2011) Pollen tube energet-
751 ics: respiration, fermentation and the race to the ovule. *AoB PLANTS*
752 10.1093/aobpla/plr019
- 753 [47] Schopfer P (2006) Biomechanics of plant growth. *Am J Bot* 93: 1415-
754 1425

- 755 [48] Wei C, Lintilhac PM (2007) Loss of stability: A new look at the physics
756 of cell wall behaviour during plant cell growth. *Plant Physiol* 145:763-772
- 757 [49] Winship LJ, Obermeyer G, Geitmann A, Hepler PK (2010) Under pres-
758 sure, cell walls set the pace. *Trends Plant Sci* 15: 363-369
- 759 [50] Winship LJ, Obermayer G, Geitmann A, Hepler PK (2011) Pollen tubes
760 and the physical world. *Trends Plant Sci* 16: 353-355
- 761 [51] Zerzour R, Kroeger JH, Geitmann A (2009) Polar growth in pollen tubes
762 is associated with spatially confined dynamic changes in cell mechanical
763 properties. *Developmental Biol* 334: 437-446
- 764 [52] Zonia L, Munnik T (2007) Life under pressure: hydrostatic pressure in
765 cell growth and function. *Trends Plant Sci* 12: 90-97
- 766 [53] Zonia and Munnik (2008) Vesicle trafficking dynamics and visualization
767 of zones of exocytosis and endocytosis in tobacco pollen tubes. *J Exp Bot*
768 59, 861-873
- 769 [54] Zonia L, Munnik T (2009) Uncovering hidden treasures in pollen tube
770 growth mechanics. *Trends Plant Sci* 14: 318-327
- 771 [55] Zonia L (2010) Spatial and temporal integration of signaling networks
772 regulating pollen tube growth. *J Exp Bot* 61: 1939-1967
- 773 [56] Zonia L, Munnik T (2011) Understanding pollen tube growth: the hy-
774 drodynamic model versus the cell wall model. *Trends Plant Sci* 7: 1-6

A



B

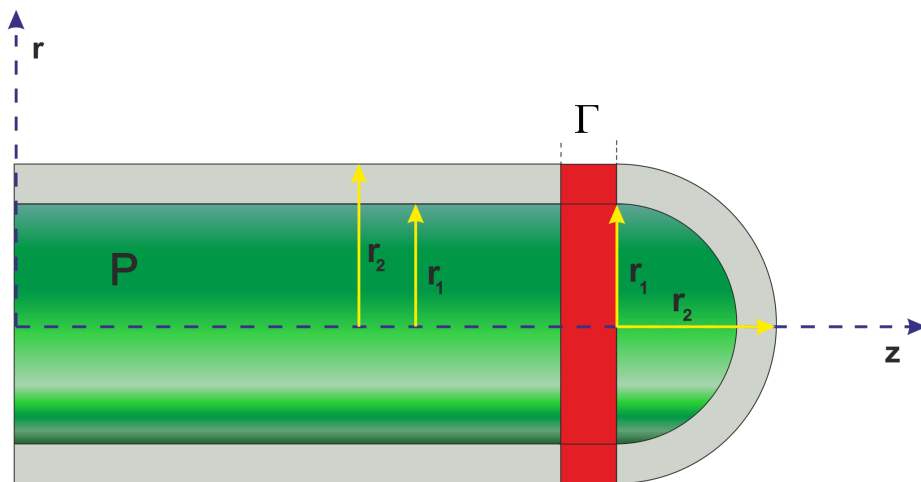


Figure 1: *Nicotiana tobaccum* pollen tube apical region. (A) Microscopic view (B) Schematic view: radii of curvature r_1 and r_2 , turgor pressure P and the investigated partition into two distinct regions (a narrow transition zone) are indicated in the chart.

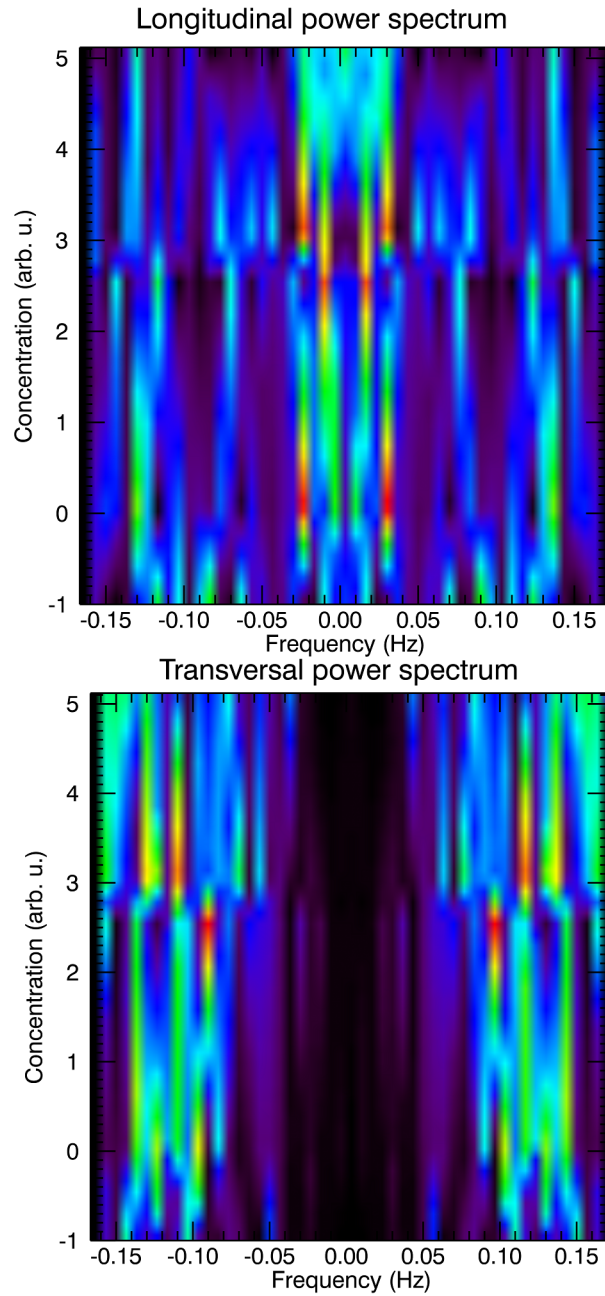


Figure 2: Density plots of the longitudinal and transversal power spectrum of *Nicotiana tabacum* pollen tube obtained from the raw experimental data, bias subtracted (Haduch and Pietruszka, 2012) by Fourier analysis, calculated by the power of the Nyquist criterion and Nyquist rate, for different osmotic environments (-1 corresponding to the hypotonic case, 0 – isotonic case, and 2.5, 3 and 5 corresponding to 25, 30 and 50 mM NaCl in hypertonic conditions, respectively). A broad, narrowing valley at the centre of the lower plot is clearly visible – low frequencies seen for longitudinal modes are shifted outwards. Red colour indicate high intensity peaks. Interpolated by DAVE, developed at NIST (Azuaq et al., 2009).

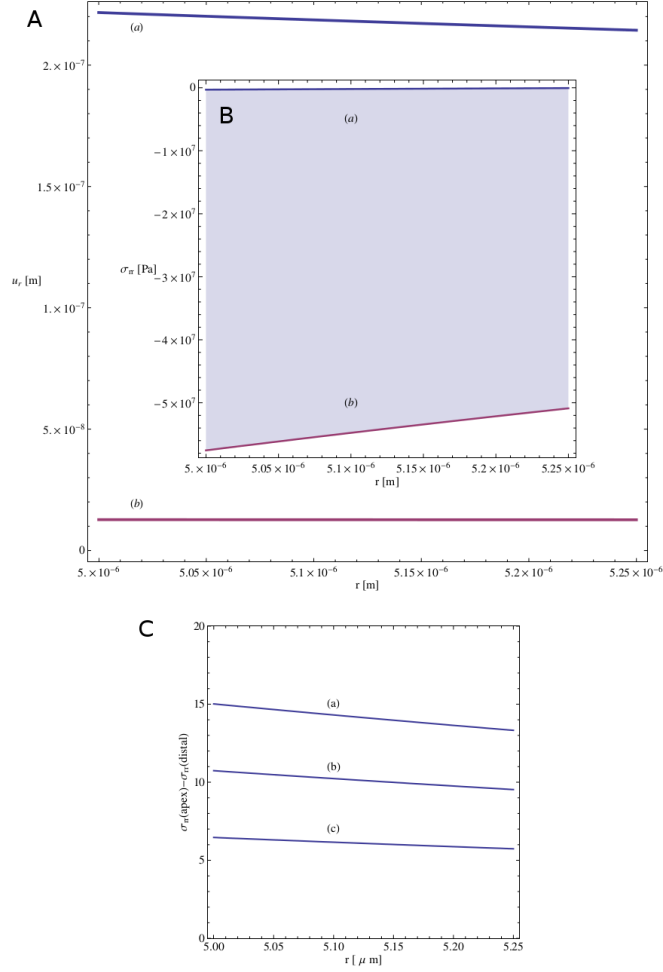


Figure 3: (A) Displacement u_r due to the effective turgor pressure \tilde{P} ($P = 0.3$ MPa, $p_{\text{ext}} = 0.05$ MPa) acting on the cell wall as a function of the radial distance r from the pollen tube long axis. Different Young modulus ϵ and Poisson coefficient ν in both subsystems: (a) $u_r = u_r^s$ for a hemispherical apex: $r_1 = 5 \mu\text{m}$, $r_2 = 5.25 \mu\text{m}$, $\nu = 0.4$, $\epsilon = 0.2$ [GPa] (b) $u_r = u_r^c$ for a cylindrical distal part: $r_1 = 5 \mu\text{m}$, $r_2 = 5.25 \mu\text{m}$, $\nu = 0.2$, $\epsilon = 1$ [GPa]. (B) Tensile stress σ_{rr} due to the effective turgor pressure \tilde{P} acting on the cell wall at the position where (a) the cylinder (shank) joins (b) the hemisphere (apex) as a function of the radial distance r from the pollen tube axis. Radial stress discontinuity between the distal wall and apical wall is proportional to the distance between the curves (a) and (b). The calculated maximum wall stress reaches about 60 MPa for the simulation parameters. The strain energy leading to oscillations is proportional to the shaded area. (C) Tensile stress difference $\sigma_{rr}(\text{apex}) - \sigma_{rr}(\text{distal})$ (in MPa) at the apex and the distal part parametrized by the changing turgor pressure P acting on the cell wall: (a) $P = 0.5$ MPa, (b) $P = 0.4$ MPa and (c) $P = 0.3$ MPa.

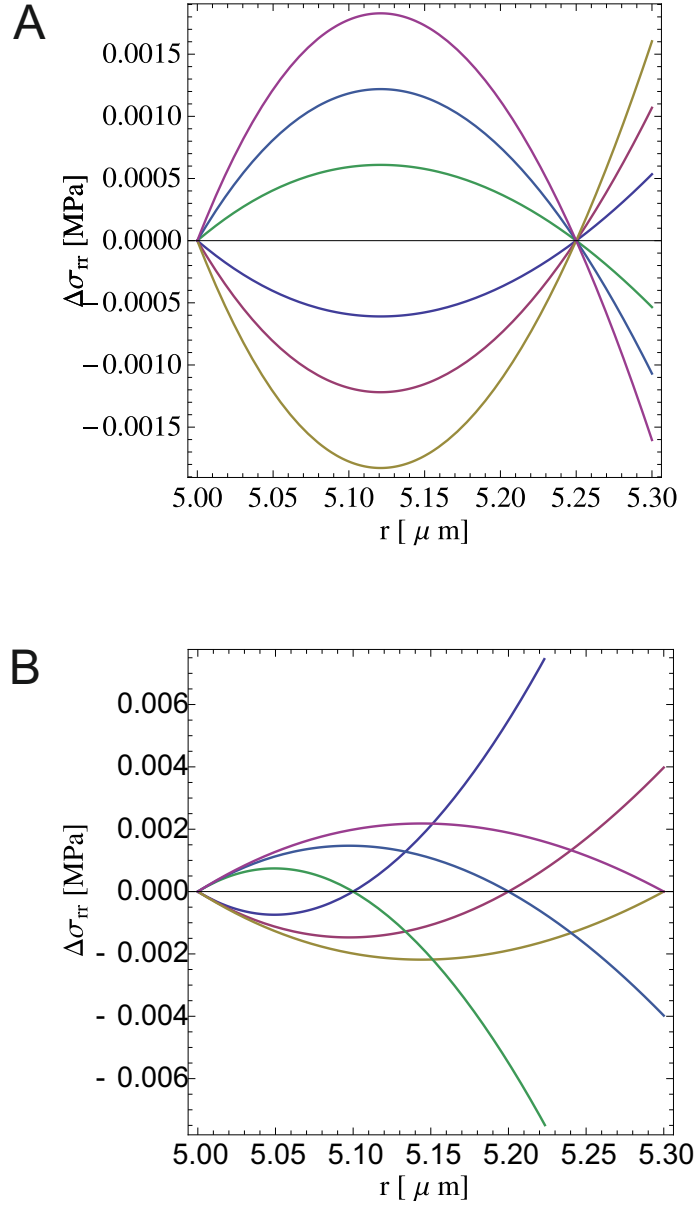


Figure 4: Tensile stress difference (A) $\sigma_{rr}^c - \sigma_{rr}^s$, upper curves, and the opposite case $\sigma_{rr}^s - \sigma_{rr}^c$, lower curves, calculated at the boundary zone between the approximately hemispherical apical and the cylindrical distal part of the growing pollen tube. Parametrisation by the turgor pressure P acting on the cell wall (upper plots): $P = 0.1$ (green), $P = 0.2$ (blue) and $P = 0.3$ MPa (violet). Remaining parameters for the respective wall geometries: $r_1 = 5 \mu\text{m}$, $r_2 = 5.25 \mu\text{m}$. (B) $\sigma_{rr}^c - \sigma_{rr}^s$, upper curves and the opposite $\sigma_{rr}^s - \sigma_{rr}^c$, lower curves, calculated at the boundary zone between the semispherical apical and the cylindrical distal part of the growing pollen tube, parametrized by the wall thickness (upper plots): $r_2 = 5.1 \mu\text{m}$ (green), $r_2 = 5.2 \mu\text{m}$ (blue) and $r_2 = 5.3 \mu\text{m}$ (violet). The inner wall radius: $r_1 = 5 \mu\text{m}$; turgor pressure $P = 0.3$ MPa.

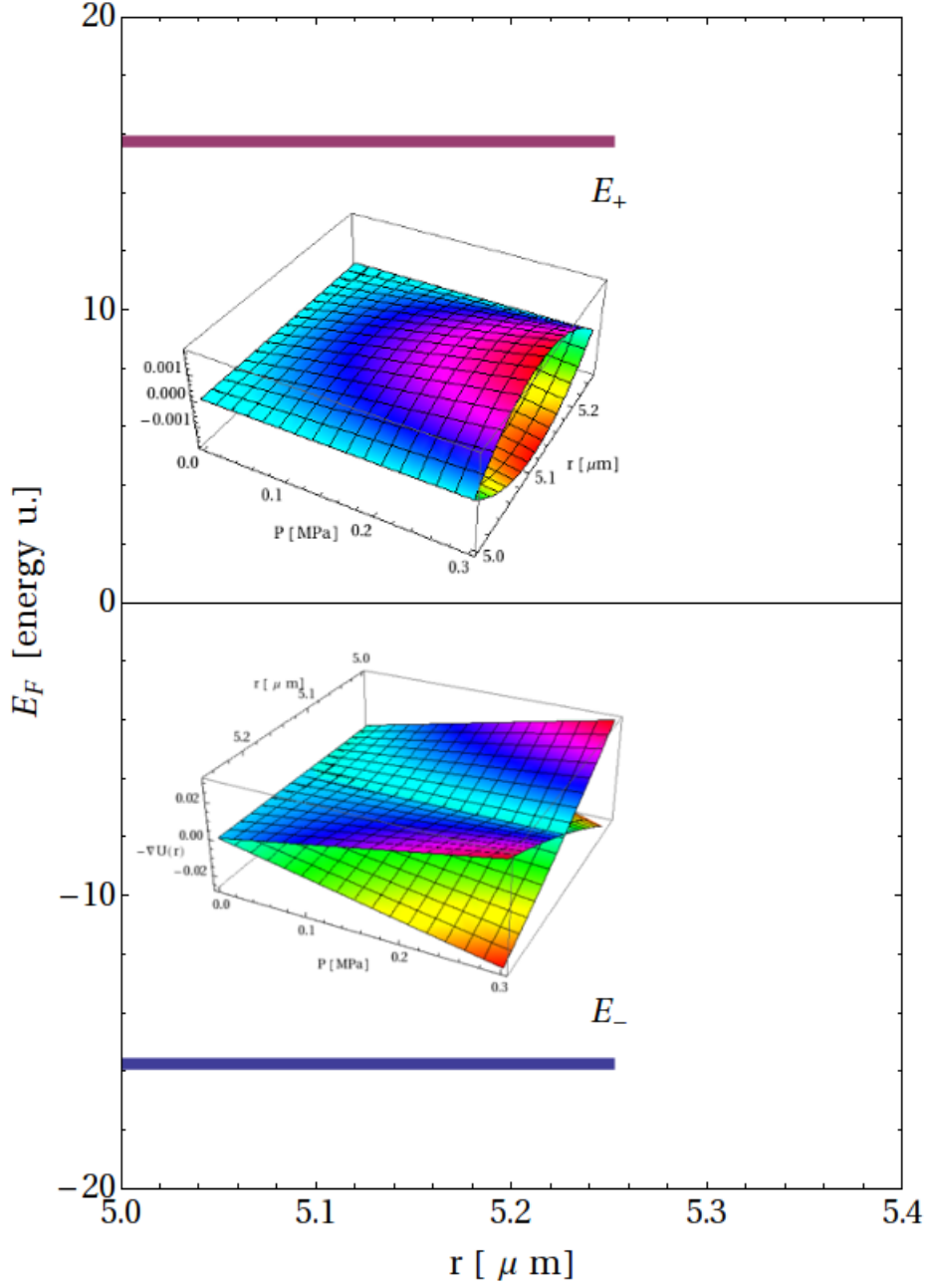


Figure 5: Frustration energy E_F splitting due to topological effects (Insets: bifurcation diagram and tensegrity force $F = -\nabla U(r)$ balance diagram) in a quasi-2D biological system – pollen tube apical region. Corresponding symmetry exchange takes place between the resonating residual energy levels $E_- \pm \delta E$ and $E_+ \pm \delta E$ of different major symmetry. Calculation performed at the transition zone between the (hemi-spherical) apical and the (cylindrical) distal part of a growing pollen tube (see Eq. (7)), at a constant turgor pressure $P = 0.3$ MPa. The inner and the outer wall radius in both subsystems read: $r_1 = 5 \mu\text{m}$, $r_2 = 5.25 \mu\text{m}$ (wall thickness ~ 250 nm), respectively. The dispersion of each energy level $\delta E \cong 0.0003$.

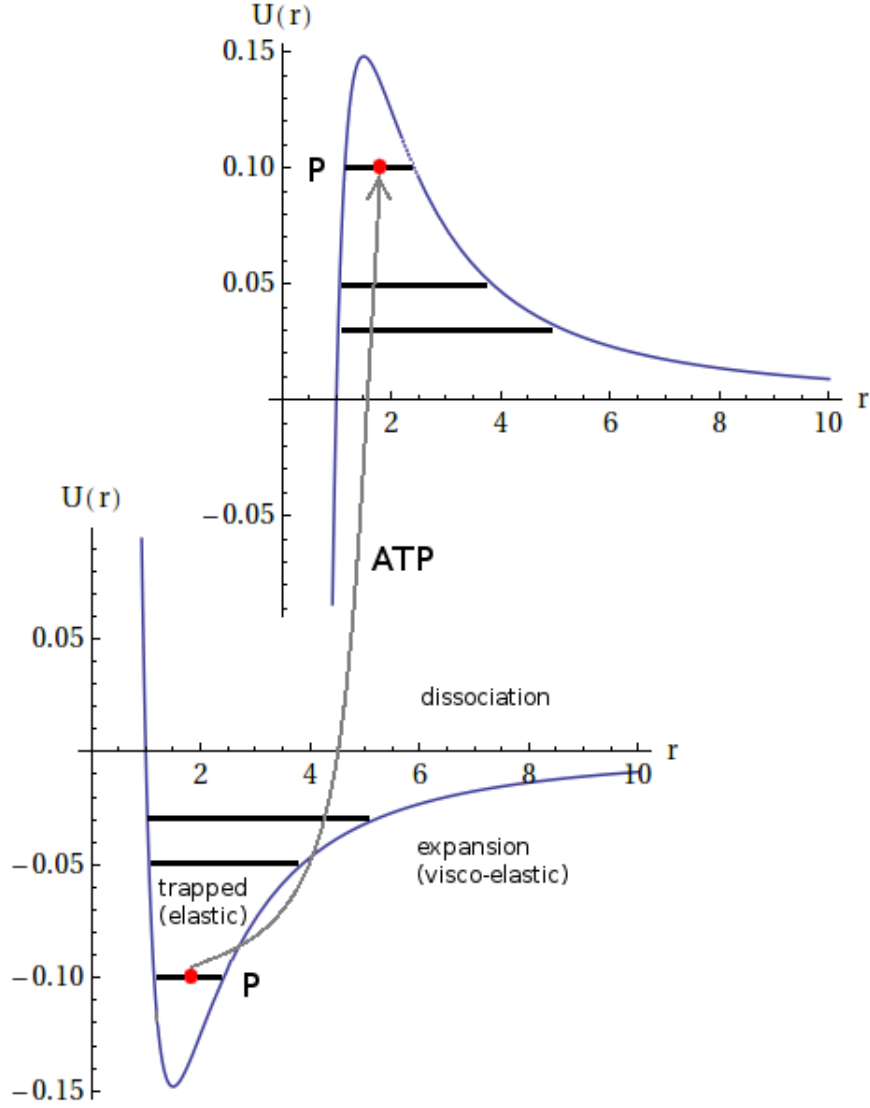


Figure 6: Two branches of the anharmonic potential energy (frustration potential) $U_{\pm}(r) \propto \pm \frac{\alpha}{r^3} \mp \frac{\beta}{r^2}$, possibly leading to pollen tubes growth rate oscillations, as a function of wall constituting molecules separation r . (Here: $\alpha = \beta = 1$; in general the coefficients α and β are linear in P , see Appendix 1). Oscillations take place between U_- and U_+ potential energy level (by tunneling through symmetry change) yielding ω , while the amplitude is determined by the actual pressure P level, in accord with experiments (Kroeger and Geitmann, 2011a; Kroeger et al., 2011).

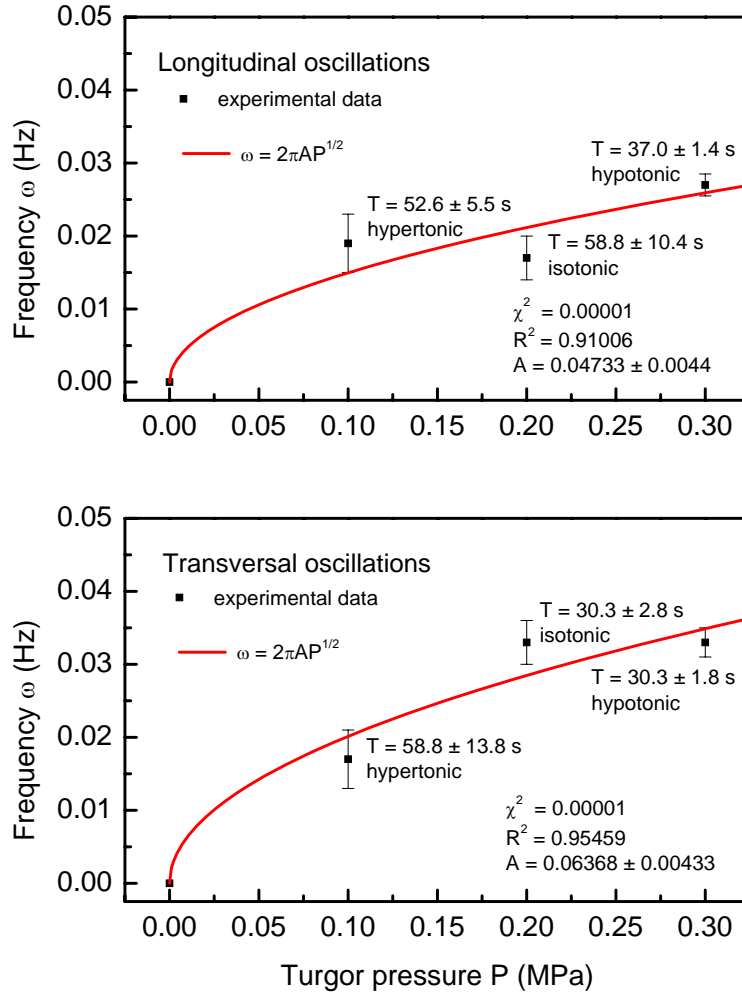


Figure 7: Least square fit of the experimental data (ω) as a function of turgor pressure P for hypertonic (25 mM NaCl), isotonic and hypotonic (hypo-osmotic stress induced by the addition of water to the gel cultures) treatment of *Nicotiana tobaccum* pollen tube (Haduch and Pietruszka, 2012) fitted to the square root function (Appendix 1) derived in this paper ($\omega = 2\pi A\sqrt{P}$; [A^2] = m/kg). Stable turgor values correspond to those ranging between 0.1 and 0.4 MPa, which has been recorded using a turgor pressure probe, (Benkert et al., 1997). The initial point (0,0) added 'by hand' in the chart is exact – the pollen tube will not oscillate ($\omega = 0$) for the vanishing turgor pressure ($P = 0$).